Reconstructing Ocean-Plate stratigraphy (OPS) to Understand Accretionary Style and Mélange Fabric: Insights from the Bangong-Nujiang Suture (Tibet, China)

Min Zeng[1,2,3], Ruisi Zhang[1], Si Chen[2], Xinyu Liu[2], Chenwei Li[2], Frank R. Ettensohn[4], and Lidong Bie[5]

[1]School of Earth Sciences, Yunnan University, Kunming 650500, China

[2]College of Earth Sciences, Chengdu University of Technology, Chengdu 610059, China

[3]Key Laboratory of Sanjiang Metallogeny, Resources Exploration & Utilization, Ministry of Natural Resources, Kunming 650051, China

[4]Department of Earth & Environmental Sciences, University of Kentucky, Lexington, KY 40506-0053, USA

[5]Geophysical Institute (GPI), Karlsruhe Institute of Technology, Karlsruhe, Germany

Corresponding authors: Min Zeng (zengmin.inter@gmail.com); Ruisi Zhang (cheerings@126.com)

Key Points:

- OPS enables tracking subduction-accretion processes in space and time and interpreting accretionary diversity and mélange fabric.
- Three types of topography on sediment-rich lower plate, recognized in OPSs, induced the accretion of distinct litho-structural assemblages.
- Thick, pervasive shear-related broken formations in accretionary complex represent shadow zones trailing subducted seamount.

Abstract

Ocean-plate stratigraphy (OPS) refers to the lithostratigraphic column atop an ocean plate, which becomes scraped off during subduction and preserved in accretionary complex (AC). Herein, based on structural, stratigraphic and geochronological studies of ACs from the Bangong-Nujiang suture, we demonstrate that OPS can facilitate interpreting structural and compositional heterogeneities in ACs. Careful correlation of OPSs reveals that, on the overall sediment-rich lower plate, three types of basement topography correspond to the accretion of distinct litho-structural assemblages. In particular, subduction of the major, high-relief Zhonggang seamount eroded the earlier margin and was subsequently accreted as coherent seamount slices. In contrast, subduction of the lower-relief, Gaize seamount halted frontal accretion of trailing sediments, which were dragged downward to the seismogenic depth and underplated as pervasive, shear-related broken formations. Such broken formations may fingerprint the former subduction of lower-relief seamount for other fossil ACs.

Plain Language Summary

Subduction of ocean plates is an important process on Earth. During subduction, the ocean-floor materials can be peeled off and become preserved above the subduction zone in a setting called the accretionary wedge. These ocean-floor materials record the stacking pattern of rock layers on the ocean plate, which is recognized as ocean-plate stratigraphy. In this study, based on careful examination of the ocean-plate stratigraphy from different areas within a fossil accretionary wedge in central Tibet, topographic and compositional variations on top of an ocean plate before subduction are restored to explain the deformation pattern of this accretionary wedge. In particular, subduction of a major seamount, which had a significant height above the sea floor, caused erosion to an earlier wedge and then added well-bedded rock units, scraped from the

seamount, onto the wedge. In contrast, a lower-relief seamount, which was largely buried in sediments, subducted deeper into the earthquake-generating depth before peeled-off in the subduction zone. Sediments trailing this seamount was dragged into a similar depth, becoming chaotic rock units, characterized as pervasive “block-in-matrix” fabrics due to prolonged subduction-related deformation. Such pervasively deformed sediments may be used to identify former seamount subduction in other on-land accretionary wedges.

1 Introduction

Accretionary wedges are tectonic settings overriding subduction zones and generally show broad structural diversity, which, in first order, is reflected in tectonic accretion or erosion (Clift and Vannucchi, 2004). Therein, the accreted materials can involve variable amounts of oceanic basement or trench-fill sediments, which occur as either coherent units or mélanges (Meneghini et al., 2009). Wedge diversity is further complicated by the fact that mélanges may result from either sedimentary, tectonic or diapiric mechanisms, or a combination thereof (Festa et al., 2012). A synthesis of modern subduction zones demonstrated that the wedge diversity is fundamentally controlled by the nature of the lower plate, particularly oceanic-basement topography and volume of sediments (Clift and Vannucchi, 2004). However, in exhumed, on-land accretionary complexes (ACs), deciphering these past lower-plate parameters is challenging.

Seaward-vergent thrust sheets are the architectural units of many ACs and develop by sequential scraping of the uppermost layers from a subducting plate. Stacking order of the layers is termed ocean-plate stratigraphy (OPS) (Wakita, 2012), which is likely the only preserved record of a subducted plate regarding relative thicknesses of trench sediments and oceanic basement. Therefore, reconstructing OPS and comparing it with associated accretionary features may reveal causal links between the lower-plate conditions and accretionary styles and clarify formative conditions of different mélange fabrics. However, such application of OPS is rare.

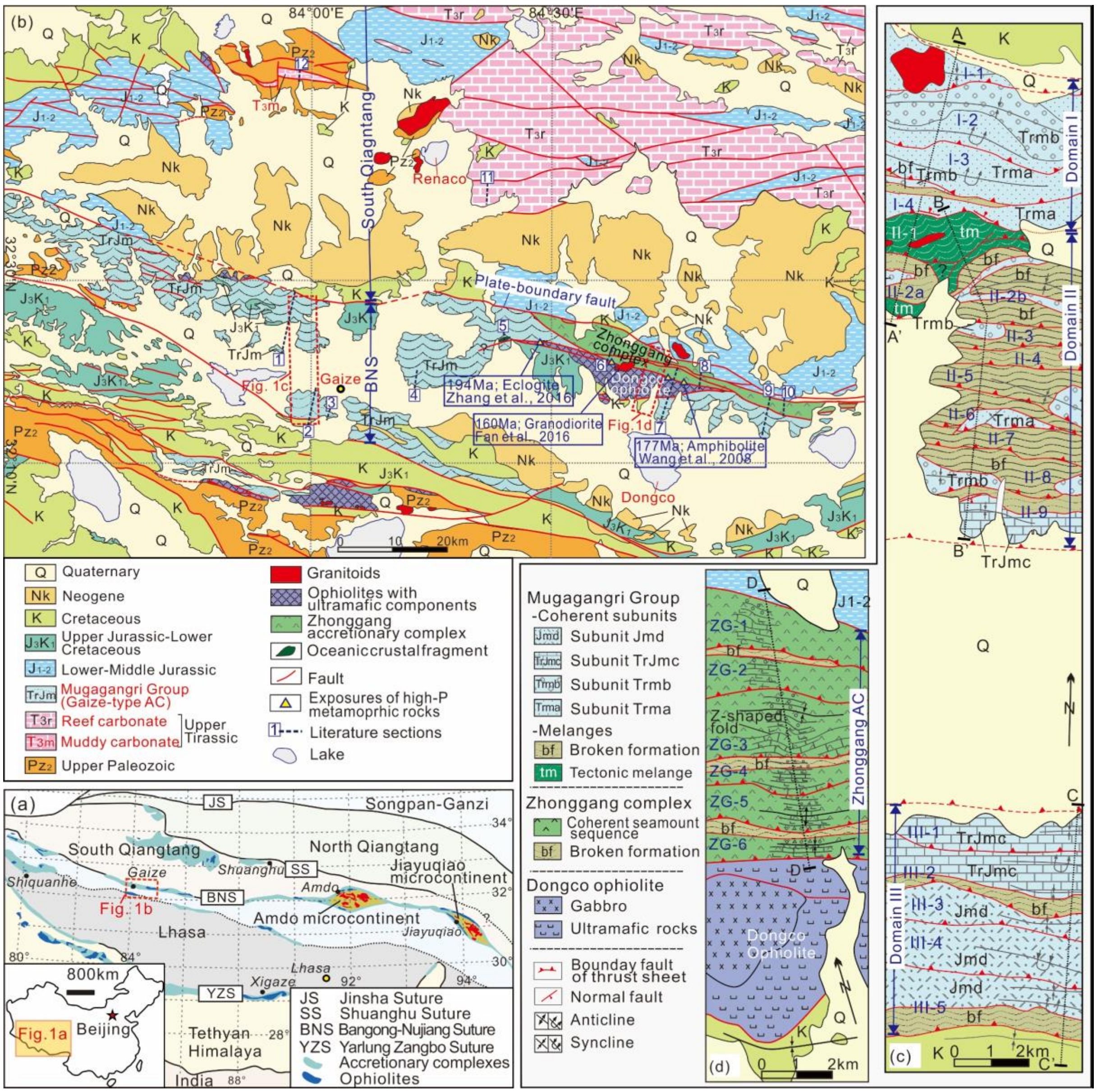

Figure 1. (a) Schematic tectonic map of the Tibetan Plateau (Zhu et al., 2013). (b) Geological map of the Gaize-Dongco area (after Zeng et al., 2006; Kapp et al., 2005). Numbered sections (1-12) are from Zeng et al. (2016), Li et al. (2017), Fan et al. (2014, 2016, 2018), Peng et al.

(2016), Chen et al. (2006), Chen (2015) and Bo et al. (2017). (c-d) Updated geologic maps of the Gaize and Dongco areas, respectively.

The Bangong-Nujiang suture (BNS) in Tibet (Fig. 1a) records birth and demise of the Meso-Tethys ocean, important episodes during Gondwana dispersal and Asian accretion (Metcalf, 2013). Key information of the BNS is carried by widespread ACs (Fig. 1a-b; Zeng et al., 2016), which, however, show dramatic variations in structure and composition that are still poorly understood. Therefore, we studied representative ACs in the Gaize-Dongco area (Fig. 1b). The results illustrate that detailed examination of OPSs enables the tracking of timing and nature of former subducting plates as well as the interpretation of associated accretionary style and mélange fabric.

2 Geological Setting

The Tibetan Plateau consists of Gondwana-derived terranes that drifted across the Tethys and amalgamated onto Eurasia along major ophiolite-bearing suture zones (Fig. 1a; Metcalf, 2013). The BNS, bounding the South Qiangtang and Lhasa terranes, is characterized by abundant flysch sequences and ophiolitic mélanges, which were considered as ACs accreted to South Qiangtang during northward Meso-Tethyan subduction. However, the timing of subduction initiation remains debated, and was suggested to be in the Late Triassic (Zeng et al., 2016) or Early to Middle Jurassic (Zhang et al., 2012; Kapp and DeCelles, 2019).

In the Gaize-Dongco area, the BNS, separated from South Qiangtang by a major plate-boundary fault, displays salient along-strike variation in accretionary style (Fig. 1b). The BNS near Gaize is mapped as the Mugagangri Group (MG), a flysch-dominated AC (Fig. 1b-c).

Detailed provenance studies demonstrated that the MG recorded persistent Late Triassic-Early Jurassic trench sedimentation (Zeng et al., 2016; Li et al., 2017, 2021). In particular, the collisional orogeny between the North and South Qiangtang terranes following the Paleo-Tethys closure was broadly coeval and contributed a persistent sediment supply for the MG (Li et al., 2021). Moreover, statistical analysis of >3500 detrital-zircon ages reported from the MG suggested that syndepositional arc-volcanism gradually became a significant source and the youngest detrital-zircon ages emerged as major peaks, which effectively approximate their depositional ages (Li et al., 2021).

In comparison, the Dongco area is dominated by ophiolitic units, namely the Zhonggang AC (ZAC) and Dongco ophiolite (DO), which are separated by a high-pressure metamorphic shear zone enclosing Early Jurassic eclogites (Fig. 1b). Basalts and carbonates predominate in the ZAC, representing remnants of a subducted seamount. The basalts show ocean-island basalt-like geochemical features (enriched light rare-earth elements; positive Nb-Ta anomalies; Fan et al., 2021). The ZAC was claimed to be Early Cretaceous in age (Fan et al., 2014), whereas other authors suggested that this age represents a later magmatic overprint during the South Qiangtang-Lhasa collision (Zhu et al., 2016). The DO comprises a full sequence of ultramafic to mafic rocks (Wang et al., 2008). Inconsistent dating results (Late Triassic, Jurassic, or Early Cretaceous) were also reported for the DO (summarized in Li et al., 2021). Nevertheless, the ZAC and DO are both unconformably overlain by Upper Jurassic-Early Cretaceous clastic rocks and intruded by ~160 Ma granitoids (Fig. 1b; Zeng et al., 2006; Fan et al., 2016). The superposition relationships indicate that their generation and emplacement were highly unlikely to occur after ~160 Ma.

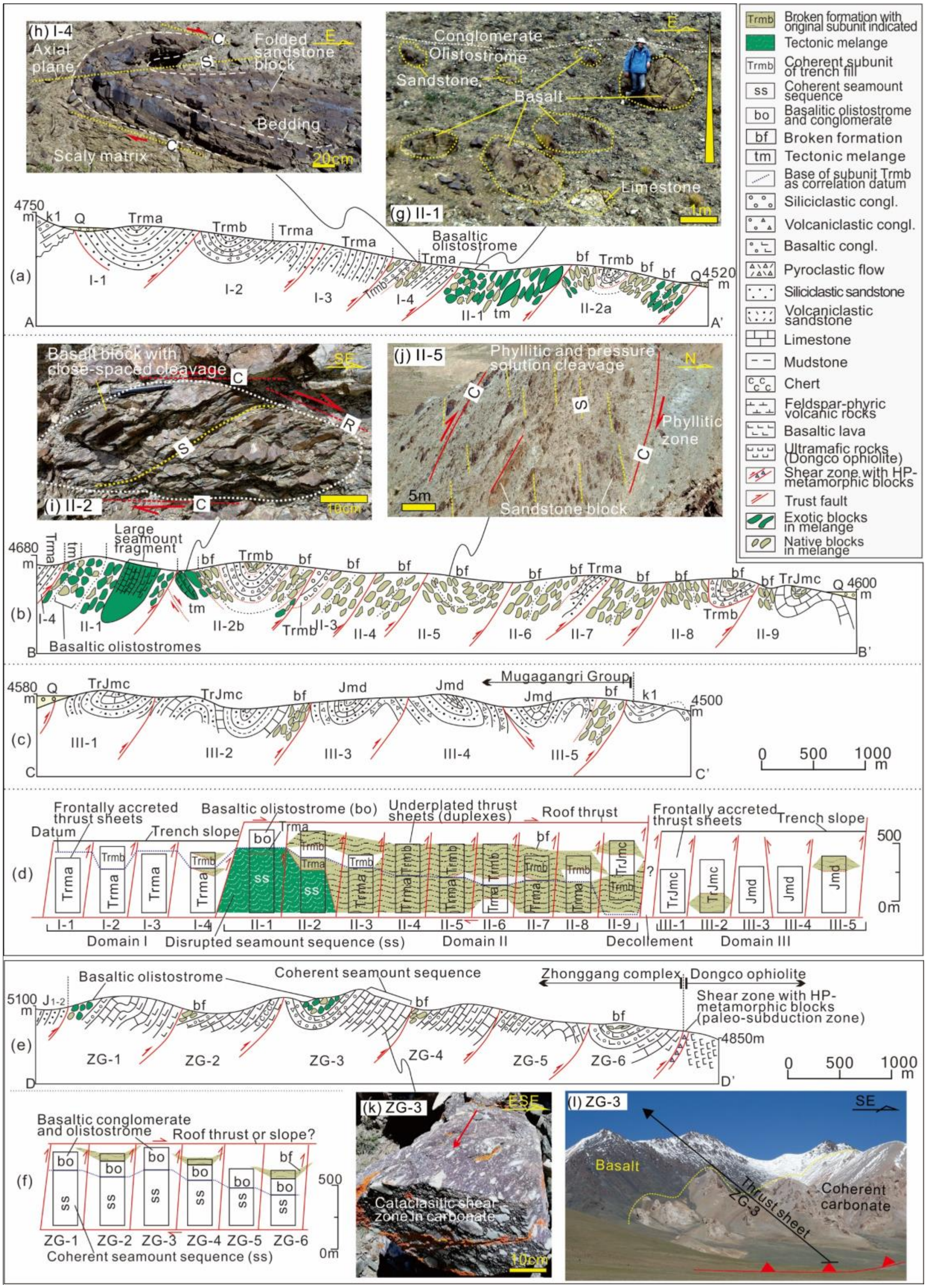

118

119 **Figure 2.** Cross-sections through the Gaize (a-c) and Zhonggang (e) ACs, and photographs of

120 key structural and lithological features (g-l). See localities for sections A-A’ to D-D’ in Fig. 1c-d.

(d) and (f) are simplified OPS columns for the thrust sheets and their correlations. (g) Basaltic olistostrome with low aspect ratios of blocks and poorly-developed shear fabric. (h) Broken formation intercalated in domains I and III, characterized by scaly matrix and ductily-deformed sandstone blocks. (i) Basaltic blocks of tectonic mélange with finely-laminated phyllitic cleavage. (j) Pervasive broken formation in domain II, characterized by cataclasis and pressure solution of angular blocks, and phyllitic matrix. Mélange fabrics of (h-j) indicate consistent top-to-the-SE shear senses. (k) Cataclastic shear zone in carbonate of basal thrust sheet ZG-3, indicating southward overthrusting. (l) Coherent seamount sequence from the Zhonggang AC.

3 Materials and Methods

Field mapping and section measurement revealed detailed structural and lithological features of the BNS in the Dongco-Gaize area (Fig. 1-2): (1) consistent south-vergent thrust sheet imbrication, (2) stratified turbiditic flysch sequence (trench fill) and basalt-chert-carbonate succession, and (3) widespread mélanges. These are essential characteristics of ACs that contain OPS-preserving packages scraped off from a subducted plate (e.g., Wakita, 2012; Wakabayashi, 2017).

Herein, stratigraphic relationships within single thrust sheet were restored based on following criteria: (1) overall younging from a basalt-chert-carbonate unit to a flysch-type trench fill (e.g., Wakita, 2012); (2) depositional ages of trench fills constrained by detrital-zircon geochronology (see methods in Text S1 in the supporting information) and published geochronological data (Fig. 3); (3) mesoscale way-up structures (e.g., Fig. S3); and (4) stratigraphic order of four subunits (Tr*ma*, Tr*mb*, TrJ*mc*, and J*md* in ascending order) identified from the trench fills (Fig. 3; Zhang and Zeng, 2018). On these grounds, a tectonostratigraphic column was established to represent the OPS of each thrust sheet (Fig. 2). The OPSs were correlated and restored to original ocean-floor setting for interpreting related subduction-accretion processes.

Extensional crack-seal veins (Fig. S2) preferentially occur within the blocks of the domain-II mélanges. These veins, sub-perpendicular to long axes of blocks or in web-like pattern, increase in abundance and widen toward to the necks of blocks, suggesting they were likely concurrent to the mélange formation (Fig. S2; Matsumura et al., 2003). These veins were collected for fluid-inclusion analysis to acquire their fluid-trapping temperatures (see methods in Text S2), which were demonstrated as effective estimates to the thermal conditions of mélange formation (Matsumura et al., 2003).

4 Results

4.1 Lithologic and structural characteristics

The Gaize AC is subdivided into three deformation domains (I, II and III from north to south; Fig. 1c). Domains I and III are mainly thrust sheets of coherent, flysch-type trench fills (Fig. 2a-d). In contrast, mélanges of typical block-in-matrix fabric predominate in domain II (Fig. 2a-d). A major part of the mélanges is broken formation (Fig. 1c; thrust sheets II-2 to -9), which denotes tectonically disrupted trench fills with recognizable stratigraphic identity (Onishi et al., 2001). Tectonic mélanges, containing tectonically fragmented blocks of "exotic" basalt, chert and carbonate, only occur in thrust sheets II-1 and -2 (Fig. 1c). These two types of mélanges were likely developed during subduction and termed as subduction mélanges (Ujiie et al., 2018). Despite tectonic mixing, the primary layering of rocks, reflecting OPS, can be restored from these subduction mélanges (Fig. S3). The third type of mélange (olistostrome) has a sedimentary origin and is differentiated by the low aspect ratios of blocks, poorly developed shear fabric and local gradation into conglomerate (Fig. 2g; Clarke et al., 2018). Stratigraphic relationships among separate blocks cannot be restored for the olistostromes.

Three deformation phases are recognized from the ACs. The first phase is best exemplified in Domain II by the systematic shear fabrics of the subduction mélanges, which show consistent strike-slip components (top-to-the-SE; Figs. 2h-j). A second phase is reverse dip-slip dominated, reflected in the E-W trending, map-scale fold-thrust sheets (Fig. 1-2). Its superposition on the first phase is manifested by that the folding overturned the strike-slip-dominated mélange fabrics (Fig. S3). Similar deformation features and sequence have been recognized in other well-defined ACs, and explained by comparable subduction-accretion processes (Onishi et al., 2001; Vannucchi et al., 2006). Herein, the first-phase subduction-mélange fabrics are attributable to underthrusting-related shear as sitting atop the subducting slab. Their strike-slip components likely reflect an oblique subduction vector to the NW (Onishi et al., 2001). Subsequently, the underthrusting top layers may be peeled off and underplated, as the subduction decollement can migrate into interior of the slab, a process termed "step-down" and recognized at both active and fossil subduction zones (Park et al., 2002). The second-phase deformation most probably resulted from this process, which underplated the trench-parallel, fold-thrust sheets (Kimura et al., 2007). In domains I and III, the predominance of coherent stratigraphy (Fig. 2d) is likely due to less-distant underthrusting that was terminated by frontal accretion (Meneghini et al., 2009). The third deformation phase is characterized by distributed normal faulting and is frequently observed near the boundary between domains I and II (Fig. 1c). It likely represents a later exhumation event, which juxtaposed these two domains that were originally accreted at different depths (Vannucchi et al., 2006).

The ZAC also comprises south-vergent thrust sheets (ZG-1 to ZG-6), in which coherent sequences of basalt and carbonate predominate (Fig. 2e-f). Shear-related block-in-matrix fabrics occur in a few flysch intervals. These shear fabrics, along with the Z-shaped asymmetric folds observed at map scale (Figs. 1d, S3), also indicate a dextral strike-slip component and likely correspond to the underthrusting-related, first-phase deformation (Fukui and Kano, 2007). Near the bases of thrust sheets, carbonates are preferentially faulted, and the asymmetric breccias indicate reverse dip-slip shear (Fig. 2k), probably representing the accretion-related, second-phase structures.

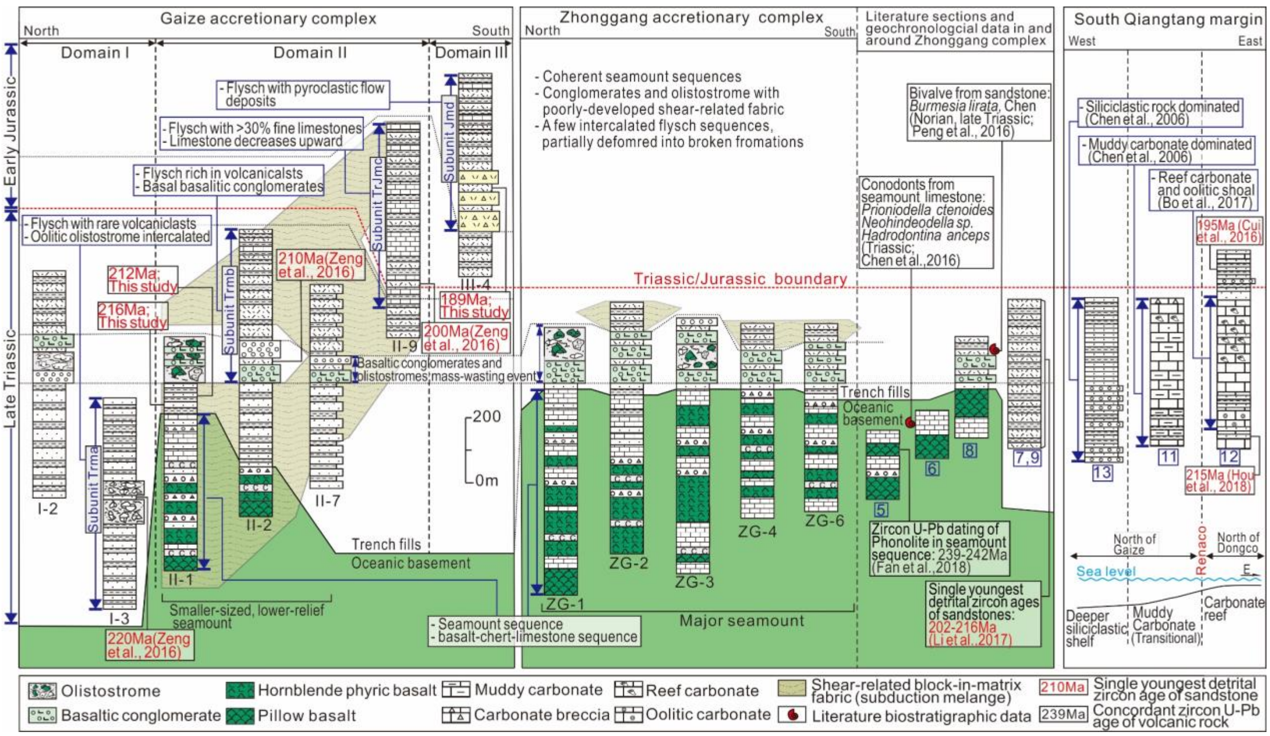

Figure 3. Details of representative OPSs and their correlation. Sections from the South Qiangtang margin show along-strike lithofacies variation. Localities and references for numbered sections refer to Figure 1b, except that section 13, located further west, is from Chen et al. (2006).

4.2 Ocean-plate stratigraphy

In the Gaize AC, the OPSs of domains I and II mainly comprise Upper Triassic flysch-type trench fills (subunits Tr*ma* and Tr*mb*), whereas the Lower Jurassic, subunits TrJ*mc* and J*md*, only occurs in thrust sheet II-9 and domain III (Fig. 2-3). Notably, the basal part of subunit Tr*mb* (~210Ma) is a conglomeratic to olistostromal interval containing sandstone, and exotic basalt and chert clasts (Fig. 3). This interval shows stable stratigraphic position, making it an ideal marker bed for correlation (Fig. 3).

OPSs of the tectonic mélange-dominated thrust sheets (II-1 and -2) consist of, in ascending order, basalt-chert-carbonate successions, thinner flysch sequences, and olistostromes and conglomerates with components similar to the marker bed (Figs. 3, S3). Importantly, our new detrital-zircon geochronology for sandstones from the flysch (II-1) yielded prominent youngest-zircon-age peaks at ~216 Ma and ~212 Ma, which can be used with confidence to approximate their depositional ages (Figs. S1, 3; Text S1). The age spectra overall resemble other previous trench-fill samples, consistent to a Qiangtang provenance (Fig. S1; Text S1). These facts suggest that the flysch and overlying coarse interval are trench fills equivalent to subunits Tr*ma* and Tr*mb*, in terms of both depositional age and provenance (Fig. 3). The reduced flysch thicknesses indicate that they were deposited on a lower-relief seamount, which is represented by the basal basalt-carbonate interval (Fig. 3).

The Zhonggang OPSs also consist of lower basalt-carbonate successions overlain by olistostromes and conglomerates (Fig. 3). The carbonates are thick to massive bedded (Fig. 2l), reportedly containing scleractinian-coral reef components (Zeng et al., 2006; Chen, 2016). Volcanic breccias common in the lower successions comprise almost purely basalt clasts (Fig. S3), likely primary volcaniclastic deposits within an intra-oceanic seamount (Buchs et al., 2011, 2018). In contrast, the upper conglomerates and olistostromes contain additional, abundant sandstone clasts, strikingly similar to the marker bed. Therefore, the Zhonggang OPSs are likely correlative with those on thrust sheets II-1 and -2 from Gaize. Supporting this correlation are multiple lines of evidence (Figs. 1b, 3): (1) the Norian index bivalve, *Burmesia lirata* and a Triassic conodont assemblage were recently reported from the ZAC (Peng et al., 2015; Chen, 2016); (2) a similar basalt-carbonate sequence near the ZAC was dated as Middle Triassic in age (Fan et al., 2018); and (3) the eclogites from the shear zone bounding the ZAC were suggested to start exhumation at ~194 Ma and represent a paleo-subduction, which initiated no later than ~215 Ma (Zhang et al., 2016) and more likely generated a Late Triassic AC.

In combination, we suggest that the Gaize and Zhonggang ACs are composed of equivalent OPSs, including Middle-Late(?) Triassic oceanic basement and Late Triassic trench fills (Fig. 3). The rarity of flysch-type trench fills in the ZAC, along with possible reef carbonates, suggests that the oceanic basement comprised a much larger seamount, in height and extent, than that subducted at Gaize.

4.3 Deformation condition

In domains I and III, the overall coherence of trench fills suggests that they were frontally accreted near the deformation front (Meneghini et al., 2009). A few horizons of broken formation are intercalated, and characterized by scaly cleavage, sandy blocks with smooth outlines, and the general absence of brittle deformation (Figs. 2a, h). Such broken formations were commonly developed by independent particulate flow before full lithification, supporting a shallow deformation depth (Kimura et al., 2007).

In contrast, the broken formations in domain II are characterized by cataclasis and pressure solution of sandstone blocks, and phyllitic cleavages that pervasively overprinted earlier scaly matrix (Fig. 2j). These features indicate a deeper deformation depth in the brittle-ductile transition zone (>5km), which largely overlaps the updip edge of the seismogenic subduction zone (Niwa, 2006). In the tectonic mélanges (II-1 to -2), in addition to cataclasis (Fig. 3S), mesoscopic shear zones bordering basaltic blocks often show finely-laminated phyllitic cleavages developed by phyllosilicate (e.g., chlorite) recrystallization (Fig. 2i). These deformation fabrics reflect basalt weakening in the brittle-ductile transition zone, where shear zones preferentially fracture the basalts (Niwa, 2006). In addition, our fluid-inclusion analysis of the crack-seal veins in the Domain-II mélanges show average fluid-trapping temperatures at 143.0-180.2°C (Table S2), further supporting that the mélanges developed around the updip edge of the seismogenic zone (~150-200°C; Matsumura et al., 2003).

The thrust sheets in the ZAC are mostly coherent (Fig. 2e, l), which suggests that the rocks were not effectively fragmented, likely due to their pre-subduction lithification and less-distant underthrusting (Vannucchi et al., 2006). The reverse fault zones in the carbonates, the accretion-phase deformation, are cataclastic with angular breccias (Fig. 2k). Such carbonate cataclasis could happen at relatively shallow depth (<1.5km) (Ferraro et al., 2019). Thus, we suggest that the ZAC is constructed by slices scraped off the seamount cap along weak sedimentary layers by shallow-level accretion (Buchs et al., 2009).

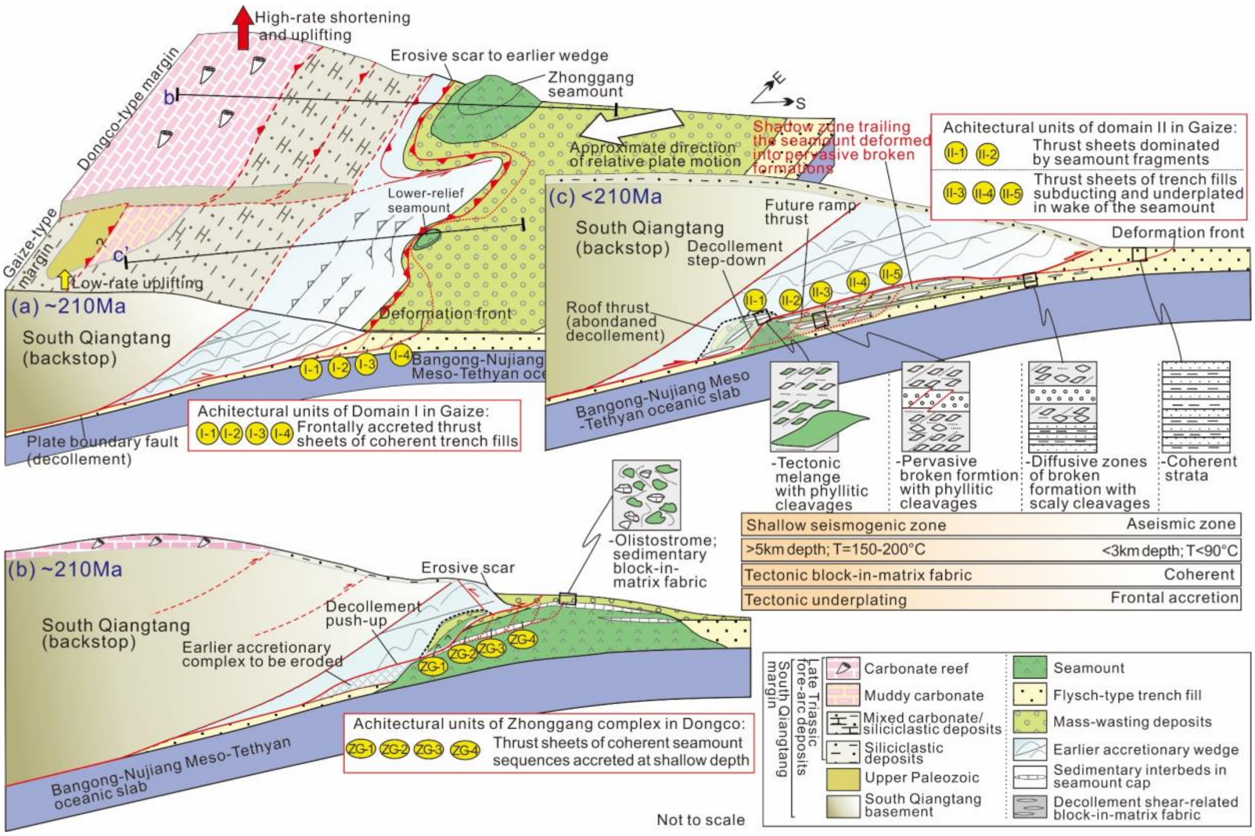

Figure 4. Speculative tectonic model explaining accretionary styles and mélange fabrics developed during the subduction of three basic types of oceanic topography, along the sediment-rich South Qiangtang margin. (a) Frontal accretion of coherent trench fills where basement asperity was negligible. (b) Tectonic erosion and shallow-level accretion of seamount slices during the major Zhonggang-seamount subduction, which generated the mass-wasting deposits and olistostrome-type mélanges. (c) The lower-relief, Gaize seamount subducted into the shallow seismogenic zone (>5km) until decollement stepped down, which underplated the seamount slices as tectonic mélanges and the trailing sediments as pervasive broken formations. Note that transect (c) is a prediction for the situation along profile c’ in the block diagram. Differential uplifting along the South Qiangtang margin is tentatively explained by subduction of different oceanic topography.

5 Discussion and Conclusions

5.1 Understanding accretionary style based on OPS

The reconstructed OPSs contain trench fills of variable thicknesses, which are most likely related to oceanic-basement topography (Fig. 3-4). In particular, the Gaize OPSs have thick (>1km) trench sediments (Fig. 3), which are typical of sediment-rich, accretionary margins (Clift and Vannucchi, 2004). This situation favored frontal accretion of coherent sediments, explaining the development of domains I and III (Fig. 4a).

In comparison, the Zhonggang OPSs comprise oceanic sequences with thin trench-fill veneers, representing a major seamount (Fig. 4b). Subduction of this seamount could erode the earlier wedge, which is supported by that the ZAC is juxtaposed directly to South Qiangtang (the backstop) along a "scar"-like, wrap-around boundary (Figs. 1b; Dominguez et al., 2000). The seamount seemingly collided with the backstop, which, we speculate, probably stopped intact subduction and facilitated off-scraping and accretion (Fig. 4b; Watts et al., 2010). The scar cuts northwesterly through the Gaize-type AC (Fig. 1b), indicating a NW-directed, oblique subduction trajectory (Dominguez et al., 2000), which confirms the underthrusting-phase shear senses inferred from the subduction mélanges (Fig. S3). Moreover, the seamount-trench collision could trigger slope failure and mass-wasting deposition, which recycled eroded-wedge and seamount materials to the trench (Ruh, 2016). Therein, this collision is well-corresponded with the widespread ~210Ma olistostromes and conglomerates, a mass-wasting interval with mixed siliciclastic and seamount-derived sediments, which overlie the seamount or sandy trench fills elsewhere (Fig. 3-4).

Notably, the domain-II OPSs (II-3 to -9) also contains thick trench fills, which were, in contrast, deformed into pervasive broken formations (Fig. 2d). They are bounded in the north by disrupted oceanic-basement sequences, which represent a lower-relief seamount (Fig. 3). As abovementioned, the broken formations and tectonic mélanges both underwent peak deformation conditions around the updip limit of the seismogenic zone, reflecting similar depths of underplating. These facts suggest that this lower-relief seamount subducted to the seismogenic depth and weakened until a decollement step-down occurred (Niwa, 2006; Fig. 4c). Seamount breakage in this process supplied exotic blocks to form the tectonic mélanges (Fig. 4c). Moreover, we envisage that the pervasive broken formations represent sediments trailing the seamount, which underwent prolonged underthrusting-related shear (Fig. 4c). Thick trench-sediment subduction following seamounts has been seismically observed in several modern subduction zones (Noda et al., 2020). Sandbox modelling also suggested that sitting in the shadow zones behind seamounts is likely a prerequisite for the deeper subduction of sediments (Noda et al., 2020). Herein, the domain-II, pervasive broken formations likely provide the first-recognized fossil record of deeper-subducted sediments trailing a seamount (Fig. 4c). Such broken formations may fingerprint former seamount subduction in other on-land ACs.

Unlike the Zhonggang seamount, the Gaize seamount apparently survived tectonic peeling at the frontal margin. We speculate that the survival was related to its lower relief, which induced uplifting but little tectonic erosion at the fontal margin, while maintaining high confining stress, low deviatoric stress and little possibility of breakage (Baba et al., 2001). In addition, the accompanying subduction of thick sediments could have enhanced fluid content, thereby reducing frictional force along the decollement (Bangs et al., 2006).

5.2 Broader Implications

Depositional age of trench sediments in ACs can approximate the timing of contemporaneous subduction (Amato and Pavlis, 2010). As abovementioned, the initial timing of Meso-Tethyan subduction remains controversial. Our reconstructed OPSs contain abundant Late Triassic trench fills (Fig. 3), which, combined with previous evidence (Zhang et al., 2016; Li et al., 2021), supports the presence of Late Triassic Meso-Tethyan subduction beneath South Qiangtang.

Distinguishing between accretionary and erosive margins is critical to our understanding of continental-crust recycling, carbon cycle, and arc magmatism. The ZAC is a clear example of subduction erosion reflected in the indentation of major oceanic relief, followed by the accretion of oceanic sequences. Similar oceanic-sequence-dominated ACs have been commonly interpreted as localized accretionary pulses along erosive margins (e.g., Clarke et al., 2018; Dumitru et al., 2010). However, the Gaize-type, trench-fill-dominated AC predominates along the BNS (Fig. 1), reflecting persistent accretion during Late Triassic-Early Jurassic time (Zeng et al., 2016). Thus, an oceanic-sequence-dominated AC may alternatively indicate localized subduction erosion along accretionary margins, joining a recent argument from the Costa Rica margin (Buchs et al., 2020). At the Costa Rica margin, long-term accretion since Eocene was likely sustained by trench sedimentation linked to local recycling of fore-arc materials during seamount collisions (Buchs et al., 2020). In comparison, the Gaize-type AC was demonstrated to develop by persistent sediment supply from broader source areas (South and North Qiangtang) maintained by active volcanism and tectonism (Li et al., 2017, 2021). We also reveal that the Zhonggang-seamount collision intercalated shorter-term mass-wasting deposition that involved more of recycled fore-arc and seamount components. As such, OPS reconstruction is anticipated to reveal processes and sources of trench-fill sequences and corresponding oceanic topography at greater spatiotemporal resolution, which may enable more detailed mass-balance evaluation at subduction zones.

It has been suggested that seamounts largely remain intact during subduction (Wang and Bilek, 2011; Kopp, 2013). However, this study shows clear evidence of seamount off-scraping (Fig. 4), enabled by lithologically weaker layers or mechanical weakening. The ZAC exemplifies that colliding with the backstop likely facilitates shallow-depth truncation of seamount slices, which may explain other global cases (e.g., the Azuero AC of Panama; Buchs et al., 2011). Moreover, regarding the function of subduction zones that recycles continental-crustal materials into the mantle, mounting evidence suggests previous overestimation of the amount of recycling (Basset et al., 2010). Here, we show that seamount subduction induced significant oceanic-material accretion at shallower-crustal depths (<10km; Fig. 4b-c), joining numerous examples reported worldwide (e.g., Buchs et al., 2011, 2020; Barbero et al., 2021). Thus, to realistically estimate continental recycling at subduction zones, these shallower circumstances must be re-evaluated, as previous studies have already emphasized lower-crustal (10-30km) underplating of subducting materials (Scholl et al., 2021).

Trench-parallel, outer fore-arc uplifts are a prominent topographic feature along most modern convergent margins, and have been attributed to either lower-crustal underplating (Menant et al., 2020) or fore-arc shortening (Morell et al., 2019). The Late Triassic South Qiangtang margin shows trench-parallel facies segmentation, with uplifts characterized by reef carbonates and low areas depositing muddy carbonates and shelf siliciclastics (Fig. 1b, 3-4). The reef carbonates occur restrictedly to the north of where the Zhonggang seamount subducted, reflecting possible spatial correspondence to contemporaneous subducting oceanic topography

(Fig. 3-4). Hence, the facts support the idea that the subduction of major oceanic topography, like the Zhonggang seamount, can drive fore-arc shortening to induce localized fore-arc uplifts, as suggested for the Costa Rica margin (Morell et al., 2019) and Nankai Trough fore-arc (Moore et al., 2015).

Acknowledgments

This study was supported by Chinese National Natural Science Foundation (No. 41102065 and 41872110) and Chengdu University of Technology (2020ZF11407). We thank the Editor and three reviewers for critical reviews and constructive comments. Data available in the Supporting Information will be uploaded to (repository).

References

Amato, J. M., & T. L. Pavlis (2010), Detrital zircon ages from the Chugach terrane, southern Alaska, reveal multiple episodes of accretion and erosion in a subduction complex, Geology, 38, 459-462.

Baba, T., T. Hori, S. Hirano, P. R. Cummins, J. Park, M. Kameyama, & Y. Kaneda (2001), Deformation of a seamount subducting beneath an accretionary prism: constraints from numerical simulation, Geophysical Research Letters, 28, 1827-1830.

Bakker, R. J. (2018), AqSo_NaCl: Computer program to calculate p-T-V-x properties in the H_2O-NaCl fluid system applied to fluid inclusion research and pore fluid calculation, Computers & Geosciences, 115, 122-133.

Bangs, N. L., S. P. Gulick, & T. H. Shipley (2006), Seamount subduction erosion in the Nankai Trough and its potential impact on the seismogenic zone, Geology, 34, 701-704.

Barbero, E., L. Pandolfi, M. Delavari, A. Dolati, E. Saccani, R. Catanzariti, V. Luciani, M. Chiari, & M. Marroni (2021), The western Durkan Complex (Makran Accretionary Prism, SE Iran): A Late Cretaceous tectonically disrupted seamounts chain and its role in controlling deformation style, Geoscience Frontiers, 12, 101106.

Bassett, D., R. Sutherland, S. Henrys, T. Stern, M. Scherwath, A. Benson, S. Toulmin, & M. Henderson (2010), Three-dimensional velocity structure of the northern Hikurangi margin, Raukumara, New Zealand: Implications for the growth of continental crust by subduction erosion and tectonic underplating, Geochemistry, Geophysics, Geosystems, 11.

Bo, J., X. Wang, J. Gao, J. Yao, G. Wang, & E. Hou (2017), Upper Triassic reef coral fauna in the Renacuo area, northern Tibet, and its implications for palaeobiogeography, Journal of Asian Earth Sciences, 146, 114-133.

Buchs, D. M., & S. A. Oemering (2020), Long-term non-erosive nature of the south Costa Rican margin supported by arc-derived sediments accreted in the Osa Mélange, Earth and Planetary Science Letters, 531, 115968.

Buchs, D. M., P. O. Baumgartner, C. Baumgartner-Mora, A. N. Bandini, S. Jackett, M. Diserens, & J. Stucki (2009), Late Cretaceous to Miocene seamount accretion and mélange formation in the Osa and Burica Peninsulas (southern Costa Rica): Episodic growth of a convergent margin, Geological Society, London, Special Publications, 328, 411-456.

Chen, Y. L., K. Z. Zhang, Y. D. Gou, & J. H. Wen (2006), 1: 250,000 geological map of Wuma region with report, Geological Survey of Sichuan Province, Chengdu.

Chen, Z. (2016), The Rock Sequences and Geochemistry Features Of The Zhonggang Ocean Island Volcanic- Sedimentary Strata, Gaize, Tibet, M.S. Thesis

thesis, 55 pp, Chengdu University of Technology Chengdu.

Clarke, A. P., P. Vannucchi, & J. Morgan (2018), Seamount chain--subduction zone interactions: Implications for accretionary and erosive subduction zone behavior, Geology, 46, 367-370.

Clift, P., & P. Vannucchi (2004), Controls on tectonic accretion versus erosion in subduction zones: Implications for the origin and recycling of the continental crust, Reviews of Geophysics, 42.

Crawford, M. L. (1981), Phase equilibria in aqueous fluid inclusions, Mineralogical Association of Canada, 4.

Dominguez, S., J. Malavieille, & S. E. Lallemand (2000), Deformation of accretionary wedges in response to seamount subduction: Insights from sandbox experiments, Tectonics, 19, 182-196.

Dumitru, T. A., J. Wakabayashi, J. E. Wright, & J. L. Wooden (2010), Early Cretaceous transition from nonaccretionary behavior to strongly accretionary behavior within the Franciscan subduction complex, Tectonics, 29.

Fan, J., C. Li, J. Liu, M. Wang, Y. Liu, & C. Xie (2018), The Middle Triassic evolution of the Bangong–Nujiang Tethyan Ocean: evidence from analyses of OIB-type basalts and OIB-derived phonolites in northern Tibet, International Journal of Earth Sciences, 107, 1755-1775.

Fan, J., C. Li, H. Wu, T. Zhang, M. Wang, J. Chen, & J. Xu (2016), Late Jurassic adakitic granodiorite in the Dong Co area, northern Tibet: Implications for subduction of the Bangong--Nujiang oceanic lithosphere and related accretion of the Southern Qiangtang terrane, Tectonophysics, 691, 345-361.

Fan, J., C. Li, C. Xie, & M. Wang (2014), Petrology, geochemistry, and geochronology of the Zhonggang ocean island, northern Tibet: implications for the evolution of the Banggongco--Nujiang oceanic arm of the Neo-Tethys, International Geology Review, 56, 1504-1520.

Ferraro, F., F. Agosta, E. Ukar, D. S. Grieco, F. Cavalcante, C. Belviso, & G. Prosser (2019), Structural diagenesis of carbonate fault rocks exhumed from shallow crustal depths: An example from the central-southern Apennines, Italy, Journal of Structural Geology, 122, 58-80.

Festa, A., Y. Dilek, G. A. Pini, G. Codegone, & K. Ogata (2012), Mechanisms and processes of stratal disruption and mixing in the development of mélanges and broken formations: Redefining and classifying mélanges, Tectonophysics, 568, 7-24.

Fukui, A., & K. Kano (2007), Deformation process and kinematics of mélange in the Early Cretaceous accretionary complex of the Mino - Tamba Belt, eastern southwest Japan, Tectonics, 26.

Gehrels, G., P. Kapp, P. Decelles, A. Pullen, R. Blakey, A. Weislogel, L. Ding, J. Guynn, A. Martin, N. McQuarrie, & Others (2011), Detrital zircon geochronology of pre-Tertiary strata in the Tibetan-Himalayan orogen, Tectonics, 30, 5016.

Hou, K., Y. Li, & Y. Y. Tian (2009), In situ U-Pb zircon dating using laser ablation-multi ion counting-ICP-MS, Mineral Deposits, 28, 481-492.

Ikesawa, E., G. Kimura, K. Sato, K. Ikeharaohmori, Y. Kitamura, A. Yamaguchi, K. Ujiie, & Y. Hashimoto (2005), Tectonic incorporation of the upper part of oceanic crust to overriding plate of a convergent margin: An example from the Cretaceous early Tertiary Mugi Mélange, the Shimanto Belt, Japan, Tectonophysics, 401, 217-230.

Kapp, P., A. Yin, T. M. Harrison, & L. Ding (2005), Cretaceous-Tertiary shortening, basin development, and volcanism in central Tibet, Geological Society of America Bulletin, 117, 865-878.

Kimura, G., Y. Kitamura, Y. Hashimoto, A. Yamaguchi, T. Shibata, K. Ujiie, & S. Okamoto (2007), Transition of accretionary wedge structures around the up-dip limit of the seismogenic subduction zone, Earth and Planetary Science Letters, 255, 471-484.

Kopp, H. (2013), Invited review paper: The control of subduction zone structural complexity and geometry on margin segmentation and seismicity, Tectonophysics, 589, 1-16.

Li, S., L. Ding, C. Guilmette, J. Fu, Q. Xu, Y. Yue, & R. Henrique-Pinto (2017), The subduction-accretion history of the Bangong-Nujiang Ocean: Constraints from provenance and geochronology of the Mesozoic strata near Gaize, central Tibet, Tectonophysics, 702, 42-60.

Li, S., C. Yin, C. Guilmette, L. Ding, & J. Zhang (2019), Birth and demise of the Bangong-Nujiang Tethyan Ocean: A review from the Gerze area of central Tibet, Earth-Science Reviews, 198, 102907.

Liu, D., R. Shi, L. Ding, Q. Huang, X. Zhang, Y. Yue, & L. Zhang (2017), Zircon U--Pb age and Hf isotopic compositions of Mesozoic granitoids in southern Qiangtang, Tibet: Implications for the subduction of the Bangong--Nujiang Tethyan Ocean, Gondwana Research, 41, 157-172.

Liu, Y., S. Gao, Z. Hu, C. Gao, K. Zong, & D. Wang (2010), Continental and oceanic crust recycling-induced melt--peridotite interactions in the Trans-North China Orogen: U--Pb dating, Hf isotopes and trace elements in zircons from mantle xenoliths, Journal of Petrology, 51, 537-571.

Ludwig, K. R. (2003), User's manual for Isoplot 3.6: A geochronological toolkit for microsoft excel. Berkeley Geochronology Center.

Matsumura, M., Y. Hashimoto, G. Kimura, K. Ohmori-Ikehara, M. Enjohji, & E. Ikesawa (2003), Depth of oceanic-crust underplating in a subduction zone: Inferences from fluid-inclusion analyses of crack-seal veins, Geology, 31, 1005-1008.

McCarthy, A., C. Chelle-Michou, O. M U Ntener, R. Arculus, & J. Blundy (2018), Subduction initiation without magmatism: The case of the missing Alpine magmatic arc, Geology, 46, 1059-1062.

Menant, A., S. Angiboust, T. Gerya, R. Lacassin, M. Simoes, & R. Grandin (2020), Transient stripping of subducting slabs controls periodic forearc uplift, Nature Communications, 11, 1-10.

Meneghini, F., M. Marroni, J. C. Moore, L. Pandolfi, & C. D. Rowe (2009), The processes of underthrusting and underplating in the geologic record: Structural diversity between the Franciscan Complex (California), the Kodiak Complex (Alaska) and the Internal Ligurian Units (Italy), Geological Journal, 44, 126-152.

Moore, G. F., B. B. Boston, M. Strasser, M. B. Underwood, & R. A. Ratliff (2015), Evolution of tectono-sedimentary systems in the Kumano Basin, Nankai Trough forearc, Marine and Petroleum Geology, 67, 604-616.

Morell, K. D., D. M. Fisher, & N. Bangs (2019), Plio-Quaternary outer forearc deformation and mass balance of the southern Costa Rica convergent margin, Journal of Geophysical Research: Solid Earth, 124, 9795-9815.

Nishiyama, N., H. Sumino, & K. Ujiie (2020), Fluid overpressure in subduction plate boundary caused by mantle-derived fluids, Earth and Planetary Science Letters, 538, 116199.

Niwa, M. (2006), The structure and kinematics of an imbricate stack of oceanic rocks in the Jurassic accretionary complex of Central Japan: an oblique subduction model, Journal of Structural Geology, 28, 1670-1684.

Noda, A., H. Koge, Y. Yamada, A. Miyakawa, & J. Ashi (2020), Subduction of trench-fill sediments beneath an accretionary wedge: Insights from sandbox analogue experiments, Geosphere, 16, 953-968.

Onishi, C. T., G. Kimura, Y. Hashimoto, K. Ikehara-Ohmori, & T. Watanabe (2001), Deformation history of tectonic melange and its relationship to the underplating process and relative plate motion: An example from the deeply buried Shimanto Belt, SW Japan, Tectonics, 20, 376-393.

Peng, T., X. Yang, H. Chu, & G. Lin (2015), Major Discovery on the Ocean Islands Constitutive Model and Prospecting in Gêrzê County of the Bangong Lake-Nujiang river Suture Zone: according to 1：50000 Gêrzê County (I45E021005) and other five regional Geological maps in Tibet, Geological Survey of China, 2, 12-23.

Pullen, A., P. Kapp, G. E. Gehrels, J. D. Vervoort, & L. Ding (2008), Triassic continental subduction in central Tibet and Mediterranean-style closure of the Paleo-Tethys Ocean, Geology, 36, 351-354.

Robertson, A. H. (2002), Overview of the genesis and emplacement of Mesozoic ophiolites in the Eastern Mediterranean Tethyan region, Lithos, 65, 1-67.

Roedder, E. (1962), Studies of fluid inclusions I: Low temperature application of a dual-purpose freezing and heating stage, Economic Geology, 57, 1045-1061.

Roedder, E. (1984), Fluid inclusions (Reviews in Mineralogy 12), Mineral Soc Am, Washington DC, 1–644 pp.

Ruh, J. B. (2016), Submarine landslides caused by seamounts entering accretionary wedge systems, Terra Nova, 28, 163-170.

Scholl, D. W. (2021), Seismic imaging evidence that forearc underplating built the accretionary rock record of coastal North and South America, Geological Magazine, 158, 104-117.

Shibata, T., Y. Orihashi, G. Kimura, & Y. Hashimoto (2008), Underplating of melange evidenced by the depositional ages: U--Pb dating of zircons from the Shimanto accretionary complex, southwest Japan, Island Arc, 17, 376-393.

Ujiie, K., H. Saishu, A. Fagereng, N. Nishiyama, M. Otsubo, H. Masuyama, & H. Kagi (2018), An Explanation of Episodic Tremor and Slow Slip Constrained by Crack‐Seal Veins and Viscous Shear in Subduction Mélange, Geophysical Research Letters, 45, 5371-5379.

Vannucchi, P., D. M. Fisher, S. Bier, & T. W. Gardner (2006), From seamount accretion to tectonic erosion: Formation of Osa Mélange and the effects of Cocos Ridge subduction in southern Costa Rica, Tectonics, 25.

von Eynatten, H., & I. Dunkl (2012), Assessing the sediment factory: The role of single grain analysis, Earth-Science Reviews, 115, 97-120.

Wakita, K. (2012), Mappable features of mélanges derived from Ocean Plate Stratigraphy in the Jurassic accretionary complexes of Mino and Chichibu terranes in Southwest Japan, Tectonophysics, 568, 74-85.

Wang, B., L. Wang, S. Chung, J. Chen, F. Yin, H. Liu, X. Li, & L. Chen (2016), Evolution of the Bangong--Nujiang Tethyan ocean: insights from the geochronology and geochemistry of mafic rocks within ophiolites, Lithos, 245, 18-33.

Wang, K., & S. L. Bilek (2011), Do subducting seamounts generate or stop large earthquakes? Geology, 39, 819-822.

Wang, W., J. C. Aitchison, C. Lo, & Q. Zeng (2008), Geochemistry and geochronology of the amphibolite blocks in ophiolitic melanges along Bangong-Nujiang suture, central Tibet, Journal of Asian Earth Sciences, 33, 122-138.

Xu, M., C. Li, X. Zhang, & Y. Wu (2014), Nature and evolution of the Neo-Tethys in central Tibet: synthesis of ophiolitic petrology, geochemistry, and geochronology, International Geology Review, 56, 1072-1096.

Zeng, M., X. Zhang, H. Cao, F. R. Ettensohn, W. Cheng, & X. Lang (2016), Late Triassic initial subduction of the Bangong-Nujiang Ocean beneath Qiangtang revealed: stratigraphic and geochronological evidence from Gaize, Tibet, Basin Research, 28, 147-157.

Zeng, Q. G., G. Z. Mai, & G. R. Chen (2006), 1: 250,000 geological map of Gaize region with report, Bureau of Geology and Mineral Resources of Xizang Autonomous Region, Lhasa.

Zhang, R., & M. Zeng (2018), Mapping Lithologic Components of Ophiolitic Mélanges Based on ASTER Spectral Analysis: A Case Study from the Bangong-Nujiang Suture Zone (Tibet, China), ISPRS International Journal of Geo-Information, 7, 34.

Zhang, Y., Z. Li, L. Zhu, K. Zhang, W. Yang, & X. Jin (2016), Newly discovered eclogites from the Bangong Meso--Tethyan suture zone (Gaize, central Tibet, western China): mineralogy, geochemistry, geochronology, and tectonic implications, International Geology Review, 58, 574-587.

Zhu, D., S. Li, P. A. Cawood, Q. Wang, Z. Zhao, S. Liu, & L. Wang (2016), Assembly of the Lhasa and Qiangtang terranes in central Tibet by divergent double subduction, Lithos, 245, 7-17.

Zhu, D., Z. Zhao, Y. Niu, Y. Dilek, Z. Hou, & X. Mo (2013), The origin and pre-Cenozoic evolution of the Tibetan Plateau, Gondwana Research, 23, 1429-1454.